Interplay between Pair Density Wave and a Nested Fermi Surface

Jin-Tao Jin,[1] Kun Jiang,[2,3,*] Hong Yao,[4,5,†] and Yi Zhou[2,3,1,6,‡]
[1]*Kavli Institute for Theoretical Sciences, University of Chinese Academy of Sciences, Beijing 100190, China*
[2]*Institute of Physics, Chinese Academy of Sciences, Beijing 100190, China*
[3]*Songshan Lake Materials Laboratory, Dongguan, Guangdong 523808, China*
[4]*Institute for Advanced Study, Tsinghua University, Beijing 100084, China*
[5]*State Key Laboratory of Low Dimensional Quantum Physics, Tsinghua University, Beijing 100084, China*
[6]*CAS Center for Excellence in Topological Quantum Computation, University of Chinese Academy of Sciences, Beijing 100190, China*

(Received 4 May 2022; revised 13 August 2022; accepted 20 September 2022; published 10 October 2022)

We show that spontaneous time-reversal-symmetry (TRS) breaking can naturally arise from the interplay between pair density wave (PDW) ordering at multiple momenta and nesting of Fermi surfaces (FSs). Concretely, we consider the PDW superconductivity on a hexagonal lattice with nested FS at 3/4 electron filling, which is related to a recently discovered superconductor CsV_3Sb_5. Because of nesting of the FSs, each momentum $\mathbf{k}$ on the FS has at least two counterparts $-\mathbf{k}\pm\mathbf{Q}_\alpha$ ($\alpha=1,2,3$) on the FS to form finite momentum ($\pm\mathbf{Q}_\alpha$) Cooper pairs, resulting in a TRS and inversion broken PDW state with stable Bogoliubov Fermi pockets. Various spectra, including (local) density of states, electron spectral function, and the effect of quasiparticle interference, have been investigated. The partial melting of the PDW will give rise to 4×4 and $(4/\sqrt{3})\times(4/\sqrt{3})$ charge density wave (CDW) orders, in addition to the 2×2 CDW. Possible implications to real materials such as CsV_3Sb_5 and future experiments have been discussed further.

DOI: 10.1103/PhysRevLett.129.167001

Introduction.—A pair density wave (PDW) is a superconducting (SC) state in which Cooper pairs carry finite momentum and its SC order parameter is spatially modulated without external magnetic field [1–19] (see, e.g., a recent review [20]). Such a kind of state is similar to the one proposed earlier by Fulde-Ferrell [21] and Larkin-Ovchinnikov [22] in a magnetic field above the Pauli limit. As a mother state for various descendant orders, e.g., charge density wave (CDW), loop current, and charge-4e superconductivity, PDWs have been receiving increasing attentions from diverse fields in physics [20,23]. In particular, PDWs were recently proposed as a promising candidate for explaining various interesting phenomena in cuprates and other strongly correlated systems [20,24–27].

In previous studies of PDWs, only electrons near hot spots on Fermi surfaces (FSs) can come into being finite momentum Cooper pairs and are gapped, while other parts of FSs remain gapless. In contrast, as will be revealed in this Letter, the FS nesting feature admits full PDW pairing around the FS, that will gain more condensation energy than the usual partial pairing, while in-gap quasiparticle excitations are still allowed. Thus, it would be of great interest to examine the interplay between these two, PDW and FS nesting. (Note that FS nesting was considered mostly to play a crucial role in CDW or spin-density-wave, e.g., see Ref. [28–33]).

In this Letter, we study PDW ordering in the presence of a nested FS on hexagonal lattices. We found that a time reversal symmetry (TRS) breaking the PDW state is energetically favored. Bogoliubov quasiparticle excitations, DOS, LDOS, and electron spectral function will be investigated as well as the quasiparticle interference (QPI) in scanning tunneling microscopy (STM). The implications to recently discovered kagome SC $AV_3Sb_5(A=K,Rb,Cs)$ will be discussed.

Model.—We start with a single band model on a hexagonal lattice, on which the FS is nested as illustrated in Fig. 1. The Hamiltonian takes the form

$$H=\sum_{\mathbf{k},\sigma}\xi_{\mathbf{k}}c^\dagger_{\mathbf{k},\sigma}c_{\mathbf{k},\sigma}+\sum_{\mathbf{k},\alpha}[\Delta_{\mathbf{Q}_\alpha}(\mathbf{k})c^\dagger_{\mathbf{k},\uparrow}c^\dagger_{-\mathbf{k}+\mathbf{Q}_\alpha,\downarrow}+\Delta_{-\mathbf{Q}_\alpha}(\mathbf{k})c^\dagger_{\mathbf{k},\uparrow}c^\dagger_{-\mathbf{k}-\mathbf{Q}_\alpha,\downarrow}+\text{H.c.}],\tag{1}$$

where $c^\dagger_{\mathbf{k},\sigma}(c_{\mathbf{k},\sigma})$ is the electron creation (annihilation) operator with momentum $\mathbf{k}$ and spin $\sigma=\uparrow,\downarrow$, $\xi_{\mathbf{k}}=\epsilon_{\mathbf{k}}-\mu$ is the energy measured from the chemical potential μ. $\Delta_{\pm\mathbf{Q}_\alpha}(\mathbf{k})=\Delta_{\pm\mathbf{Q}_\alpha}\exp[-(|\xi_{\mathbf{k}}|+|\xi_{-\mathbf{k}\pm\mathbf{Q}_\alpha}|)/(2\Lambda)]$ ($\alpha=1,2,3$) indicates the Cooper pairing with total momentum $\pm\mathbf{Q}_\alpha$. Here, Λ is an energy cutoff. Setting the lattice constant $a=1$, we consider $\mathbf{Q}_1,\mathbf{Q}_2,\mathbf{Q}_3=[0,(\pi/\sqrt{3})]$, $[-(\pi/2),-(\pi/2\sqrt{3})]$, $[(\pi/2),-(\pi/2\sqrt{3})]$, since they are most relevant to CsV_3Sb_5 for which experimental evidences

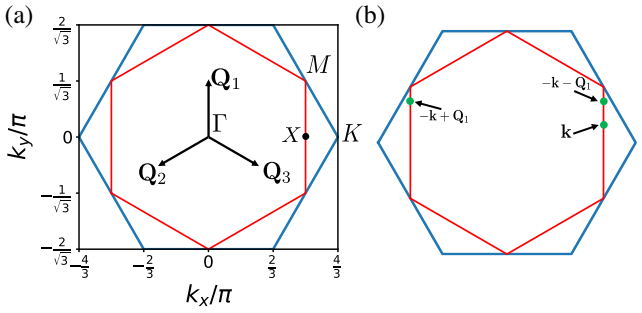

FIG. 1. First Brillouin zone (BZ) of a hexagonal lattice and nesting feature of PDWs. (a) BZ and the nested FS at 3/4 filling. The boundary of BZ is in blue, and red lines represent the FS. (b) Each $\mathbf{k}$ on a FS segment along the $\mathbf{Q}_\alpha$ direction has two counterparts $-\mathbf{k}\pm\mathbf{Q}_\alpha$ on the FS to form finite momentum ($\pm\mathbf{Q}_\alpha$) Cooper pairs.

of a period 4 PDW was recently reported [34]. As shown in Fig. 1(a), a hexagonal and nested FS can be realized by choosing μ or the electron filling properly. As a simple example, we focus on a triangular lattice, set the nearest neighbor hopping integral $t=1$, and choose $\mu=2$ (or 3/4 filling), such that $\xi_{\mathbf{k}}=-2\{\cos(k_x)+\cos[\frac{1}{2}k_x+(\sqrt{3}/2)k_y]+\cos[\frac{1}{2}k_x-(\sqrt{3}/2)k_y]+1\}$. Note that our main results will also be applicable to more generic situations, including honeycomb and kagome lattices.

From Fig. 1(b), one sees that each $\mathbf{k}$ on a FS segment along the $\mathbf{Q}_\alpha$ direction has at least two counterparts $-\mathbf{k}\pm\mathbf{Q}_\alpha$ to form finite momentum Cooper pairs. Moreover, M and X points have four momenta for pairing. These mean that the nesting feature allows full pairing in the region near the FS, which is in contrast with generic FSs without nesting.

Time reversal symmetry.—The TRS of the Hamiltonian is respected if and only if $\xi_{-\mathbf{k}}=\xi_{\mathbf{k}}$ and $\Delta^*_{\mathbf{Q}_\alpha}(\mathbf{k}+\mathbf{Q}_\alpha)=\Delta_{-\mathbf{Q}_\alpha}(\mathbf{k})$. For the aforementioned form of $\Delta_{\pm\mathbf{Q}_\alpha}(\mathbf{k})$, sufficient and necessary conditions for TRS reduce to $\Delta^*_{\mathbf{Q}_\alpha}=\Delta_{-\mathbf{Q}_\alpha}$.

The finite momentum pairing leads to a spatially varying pairing function in real space, resulting in a PDW. To be simple, we set $\Delta_{\pm\mathbf{Q}_\alpha}=\Delta e^{i\theta_\alpha}e^{\pm i(\phi_\alpha/2)}$, where Δ is real and positive, $\theta_\alpha\in(-\pi,\pi]$ and $\phi_\alpha\in(-\pi,\pi]$. Thus, the pairing function $\Delta(\mathbf{r})$ reads

$$\Delta(\mathbf{r})=2\Delta\sum_\alpha e^{i\theta_\alpha}\cos\left(\mathbf{Q}_\alpha\cdot\mathbf{r}+\frac{\phi_\alpha}{2}\right). \tag{2}$$

Commensurate PDW and descendant CDW order.—When the PDW partially melts, i.e., the $U(1)$ gauge symmetry is restored but not the translational symmetry, a descendant CDW order will arise with wave vectors $\mathbf{q}=\pm\mathbf{Q}_\alpha\pm\mathbf{Q}_\beta\neq\mathbf{0}$. These wave vectors can be classified into three sets: (B) $\mathbf{q}=\pm\mathbf{Q}_\alpha$ associated with a 4×4 CDW; (C) $\mathbf{q}=\pm2\mathbf{Q}_\alpha$ associated with a 2×2 CDW; (D) $\mathbf{q}=\pm(\mathbf{Q}_\alpha-\mathbf{Q}_\beta)$ associated with a $(4/\sqrt{3})\times(4/\sqrt{3})$ CDW [see Fig. 3(c)]. Note that the FS is nested by $\mathbf{q}=\pm2\mathbf{Q}_\alpha$ in C but not those in B or D. So that the descendant CDW order can be of 4×4 and $(4/\sqrt{3})\times(4/\sqrt{3})$, in addition to the 2×2 CDW originating from the FS nesting.

Quasiparticles.—To study quasiparticle excitations in such a PDW associated with a 4×4 folded BZ, we introduce

$$\begin{aligned}\hat{C}^\dagger_{\mathbf{k},\sigma}=(&c^\dagger_{\mathbf{k},\sigma},c^\dagger_{\mathbf{k}+\mathbf{Q}_1,\sigma},c^\dagger_{\mathbf{k}-\mathbf{Q}_1,\sigma},c^\dagger_{\mathbf{k}+\mathbf{Q}_2,\sigma},c^\dagger_{\mathbf{k}-\mathbf{Q}_2,\sigma},c^\dagger_{\mathbf{k}+\mathbf{Q}_3,\sigma},\\&c^\dagger_{\mathbf{k}-\mathbf{Q}_3,\sigma},c^\dagger_{\mathbf{k}+2\mathbf{Q}_1,\sigma},c^\dagger_{\mathbf{k}+2\mathbf{Q}_2,\sigma},c^\dagger_{\mathbf{k}+2\mathbf{Q}_3,\sigma},c^\dagger_{\mathbf{k}+\mathbf{Q}_1-\mathbf{Q}_2,\sigma},\\&c^\dagger_{\mathbf{k}-\mathbf{Q}_1+\mathbf{Q}_2,\sigma},c^\dagger_{\mathbf{k}+\mathbf{Q}_2-\mathbf{Q}_3,\sigma},c^\dagger_{\mathbf{k}-\mathbf{Q}_2+\mathbf{Q}_3,\sigma},\\&c^\dagger_{\mathbf{k}+\mathbf{Q}_3-\mathbf{Q}_1,\sigma},c^\dagger_{\mathbf{k}-\mathbf{Q}_3+\mathbf{Q}_1,\sigma}),\end{aligned}$$

and rewrite Eq. (1) in a matrix form

$$\begin{aligned}H&=\frac{1}{16}\sum_{\mathbf{k}}H_{\mathbf{k}}+\sum_{\mathbf{k}}\xi_{\mathbf{k}}\\&=\frac{1}{16}\sum_{\mathbf{k}}(\hat{C}^\dagger_{\mathbf{k},\uparrow},\hat{C}_{-\mathbf{k},\downarrow})\hat{\mathcal{H}}_{\mathbf{k}}\begin{pmatrix}\hat{C}_{\mathbf{k},\uparrow}\\\hat{C}^\dagger_{-\mathbf{k},\downarrow}\end{pmatrix}+\sum_{\mathbf{k}}\xi_{\mathbf{k}},\end{aligned} \tag{3a}$$

$$\hat{\mathcal{H}}_{\mathbf{k}}=\begin{pmatrix}\hat{D}(\mathbf{k})&\hat{\Delta}(\mathbf{k})\\\hat{\Delta}^\dagger(\mathbf{k})&-\hat{D}(-\mathbf{k})\end{pmatrix}. \tag{3b}$$

Here, $\hat{\mathcal{H}}_{\mathbf{k}}$ is a 32×32 matrix, $\hat{D}(\mathbf{k})=\mathrm{diag}\{\xi_{\mathbf{k}_i}\}$, $\mathbf{k}_i$ is the ith momentum in $\hat{C}^\dagger_{\mathbf{k},\uparrow}$, and $\hat{\Delta}(\mathbf{k})$ is a 16×16 matrix defined by $\Delta_{\pm\mathbf{Q}_\alpha}(\mathbf{k})$.

The diagonalization of $\hat{\mathcal{H}}_{\mathbf{k}}$ leads to

$$H_{\mathbf{k}}=\sum_{i=1}^{16}E(\mathbf{k})^+_i\gamma^\dagger_{\mathbf{k},\uparrow,i}\gamma_{\mathbf{k},\uparrow,i}+E(\mathbf{k})^-_i(-\gamma^\dagger_{-\mathbf{k},\downarrow,i}\gamma_{-\mathbf{k},\downarrow,i}+1), \tag{4}$$

where $E(\mathbf{k})^{+(-)}_i[i(17-i)=1,\ldots,16]$ are quasiparticle (holes) energy spectra arranged in ascending order. The particle-hole symmetry is manifested by $E(\mathbf{k})^+_i=-E(-\mathbf{k})^-_i$, which would give rise to $E(\mathbf{k})^+_i=-E(\mathbf{k})^-_i$ if the TRS was respected. $\gamma_{\mathbf{k},\uparrow(\downarrow),i}$'s are Bogoliubov quasiparticle operators, and $C^\dagger_{\mathbf{k},\uparrow,i}$ can be written in terms of them,

$$C^\dagger_{\mathbf{k},\uparrow,i}=\sum_{j=1}^{16}[u(\mathbf{k})_{ij}\gamma^\dagger_{\mathbf{k},\uparrow,j}+v(\mathbf{k})_{ij}\gamma_{-\mathbf{k},\downarrow,j}], \tag{5}$$

where $u(\mathbf{k})_{ij}$ and $v(\mathbf{k})_{ij}$ form a unitary transformation. It is easy to verify that $E(\mathbf{k})^\pm_i=E(\mathbf{k}\pm\mathbf{Q}_\alpha)^\pm_i$ and $\gamma_{\mathbf{k},\sigma,i}=\gamma_{\mathbf{k}\pm\mathbf{Q}_\alpha,\sigma,i}$, i.e., the BZ is of 4×4 folding.

$\mathbb{Z}_2$ symmetry.—It is found that there exist additional $\mathbb{Z}_2$ symmetries associated with a theorem as follows.

Theorem 1: For each α, the transformation $\Delta_{\pm\mathbf{Q}_\alpha}\mapsto-\Delta_{\pm\mathbf{Q}_\alpha}$ does not change the energy spectra of the system.

The proof of the theorem can be found in the Supplemental Material [35]. This theorem suggests a $\mathbb{Z}_2 \times \mathbb{Z}_2$ symmetry, since only two of $\mathbf{Q}_\alpha$ are independent.

Approximate $E(\mathbf{k})_1^+$.—To get insight into low energy excitations, we inspect the lowest branch of quasiparticle dispersion, $E(\mathbf{k})_1^+$, along the FS. Without loss of generality, we consider the FS segment $M - X$ [see Figs. 1(a) and 1(b)]. For each $\mathbf{k}$ on this segment and away from M and X points, it is found that only the pairings between $\mathbf{k}$ and $-\mathbf{k} \pm \mathbf{Q}_1$ are of the order of Δ, while other pairing terms are much smaller than them because of the energy cutoff. Keeping sizable terms in $\hat{\Delta}(\mathbf{k})$ and neglecting others, we find that $\hat{\mathcal{H}}_\mathbf{k}$ can be approximately decomposed into paired and unpaired parts, i.e., $\hat{\mathcal{H}}_\mathbf{k} \approx \hat{\mathcal{H}}_\mathbf{k}^p \oplus \hat{\mathcal{H}}_\mathbf{k}^f$ [35]. Therefore, $E(\mathbf{k})_1^+$ can be estimated as

$$E(\mathbf{k})_1^+ \approx \min\{E^p(\mathbf{k}), E^f(\mathbf{k})\}, \tag{6a}$$

where $E^{p(f)}(\mathbf{k})$ is the lowest non-negative eigenvalue of $\hat{\mathcal{H}}_\mathbf{k}^{p(f)}$. Straightforward algebra [35] leads to

$$E^p(\mathbf{k}) = 2\Delta \min\left\{\left|\sin\left(\frac{\phi_1}{2}\right)\right|, \left|\cos\left(\frac{\phi_1}{2}\right)\right|\right\}. \tag{6b}$$

It takes the minimum $E^p(\mathbf{k})_{\min} = 0$ at $\phi_1 = 0, \pi$ and the maximum $E^p(\mathbf{k})_{\max} = \sqrt{2}\Delta$ at $\phi_1 = \pm(\pi/2)$. Thus, the condensation of Cooper pairs will gain most energy at $\phi_\alpha = \pm(\pi/2)$. Meanwhile, $E^f(\mathbf{k})$ determined by $\hat{\mathcal{H}}_\mathbf{k}^f$ is responsible for (nearly) unpaired electrons and in-gap excitations in $E(\mathbf{k})_1^+$ as long as $E^f(\mathbf{k}) < E^p(\mathbf{k})$. The combination of $E^p(\mathbf{k})$ and $E^f(\mathbf{k})$ gives rise to $E(\mathbf{k})_1^+$, approximately.

Away from the FS or near the M or X point, other pairing terms become considerable and the simple decomposition of $\hat{\mathcal{H}}_\mathbf{k}$ does not work any more. We shall diagonalize $\hat{\mathcal{H}}_\mathbf{k}$ numerically, and study the ground state and low energy excitations. Hereafter, we set $\Lambda = 0.1$ and $\Delta = 0.02$, unless otherwise specified.

Condensation energy.—The condensation energy $E_c \equiv E_n - E_s$, that is defined by the energy difference between a SC ground state and corresponding normal state [36], has been found as $E_c = (1/N)\sum_\mathbf{k}[(1/16)\sum_{i=1}^{16}\sum_{s=\pm}\sum_{E(\mathbf{k})_i^s>0} E(\mathbf{k})_i^s - |\xi_\mathbf{k}|]$. The numerical calculation finds that $E_c[\theta_1, \theta_2, \theta_3, \phi_\alpha]$ reaches local maxima at $\phi_\alpha = \pm\pi/2$. This agrees with the above analysis of approximate $E(\mathbf{k})_1^+$ [see Eq. (6)] well. Moreover, as shown in Fig. 2(a), the PDW state acquires maximum E_c at $\phi_\alpha = \pm\pi/2$ and $\theta_2 - \theta_1 = \theta_3 - \theta_2 \equiv \pm 2\pi/3 (\mathrm{mod}\ \pi)$, breaking the TRS spontaneously. Owing to the $\mathbb{Z}_2$ symmetry theorem, $(\theta_\alpha \mapsto \theta_\alpha \pm \pi)$, the period is π, instead of 2π here.

Ginzburg-Landau free energy.—The TRS breaking and the $\mathbb{Z}_2$ symmetry can be verified in Ginzburg-Landau (GL) theory. Up to quartic order in $\Delta_{\mathbf{Q}_\alpha}$, the GL free energy can be written as [35],

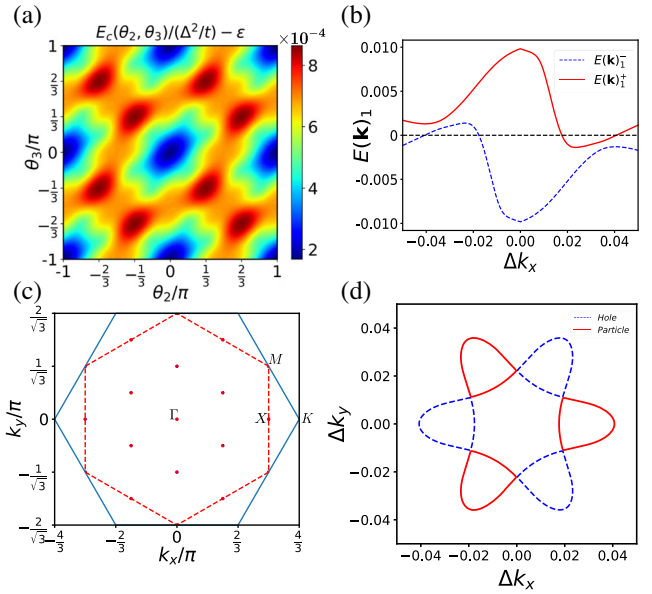

FIG. 2. (a) Condensation energy E_c (with an offset $\varepsilon = 0.993$) as a function of θ_2 and θ_3, where $\theta_1 = 0$ and $\phi_\alpha = \pi/2$ have been set [see Eq. (2)]. Maximal E_c occurs at $\theta_2 = \theta_3 - \theta_2 \equiv \pm 2\pi/3 (\mathrm{mod}\ \pi)$. (b)–(d) Energy dispersion and Bogoliubov Fermi pockets for the lowest energy state: $\phi_\alpha = \pi/2$, $\theta_1 = 0$, $\theta_2 = 2\pi/3$, and $\theta_3 = -2\pi/3$. (b) $E(\mathbf{k})_1^\pm$ around X point that are plotted along $\Gamma - X - K$. (c) Bogoliubov Fermi pockets at M and X points and their periodic replica due to the PDW. (d) Quasiparticle (hole) pocket around X point.

$$\mathcal{F}[\Delta_{\mathbf{Q}_\alpha}] = \mathcal{F}^{(0)} + \mathcal{F}^{(2)}[\Delta_{\mathbf{Q}_\alpha}] + \mathcal{F}^{(4)}[\Delta_{\mathbf{Q}_\alpha}], \tag{7}$$

where $\mathcal{F}^{(0)}$ is $\Delta_{\mathbf{Q}_\alpha}$-independent, $\mathcal{F}^{(2)} = g^{(2)}\sum_{\alpha=1}^3(|\Delta_{\mathbf{Q}_\alpha}|^2 + |\Delta_{-\mathbf{Q}_\alpha}|^2)$ with $g^{(2)} < 0$, and $\mathcal{F}^{(4)} = \mathcal{F}_0^{(4)} + \mathcal{F}_\phi^{(4)} + \mathcal{F}_\theta^{(4)}$. Here, $\mathcal{F}_0^{(4)}$ depends on $|\Delta_{\mathbf{Q}_\alpha}|$ only. $\mathcal{F}_\phi^{(4)}$ and $\mathcal{F}_\theta^{(4)}$ read

$$\begin{aligned}\mathcal{F}_\phi^{(4)} = g_\phi^{(4)}[&(\Delta_{\mathbf{Q}_1}^2)(\Delta_{-\mathbf{Q}_1}^2)^* + (\Delta_{\mathbf{Q}_2}^2)(\Delta_{-\mathbf{Q}_2}^2)^* \\ &+ (\Delta_{\mathbf{Q}_3}^2)(\Delta_{-\mathbf{Q}_3}^2)^* + \mathrm{c.c.}],\end{aligned} \tag{8a}$$

and

$$\begin{aligned}\mathcal{F}_\theta^{(4)} = g_\theta^{(4)}[&(\Delta_{\mathbf{Q}_1}\Delta_{-\mathbf{Q}_1})(\Delta_{\mathbf{Q}_2}\Delta_{-\mathbf{Q}_2})^* \\ &+ (\Delta_{\mathbf{Q}_2}\Delta_{-\mathbf{Q}_2})(\Delta_{\mathbf{Q}_3}\Delta_{-\mathbf{Q}_3})^* \\ &+ (\Delta_{\mathbf{Q}_3}\Delta_{-\mathbf{Q}_3})(\Delta_{\mathbf{Q}_1}\Delta_{-\mathbf{Q}_1})^* + \mathrm{c.c.}],\end{aligned} \tag{8b}$$

respectively, where both $g_\phi^{(4)}$ and $g_\theta^{(4)}$ are found to be positive and $\Delta_{\mathbf{Q}_\alpha}$-independent [35]. Putting $\Delta_{\pm\mathbf{Q}_\alpha} = \Delta e^{i\theta_\alpha} e^{\pm i(\phi_\alpha/2)}$ into the above leads to $\mathcal{F}_\phi^{(4)} = 2g_\phi^{(4)}\Delta^4\sum_{\alpha=1}^3\cos(2\phi_\alpha)$ and $\mathcal{F}_\theta^{(4)} = 2g_\theta^{(4)}\Delta^4[\cos(2\theta_2 - 2\theta_1) + \cos(2\theta_3 - 2\theta_2) + \cos(2\theta_1 - 2\theta_3)]$. Thus, the lowest free energy is achieved at $\phi_\alpha = \pm\pi/2$ and $\theta_2 - \theta_1 = \theta_3 - \theta_2 \equiv \pm 2\pi/3 (\mathrm{mod}\ \pi)$.

Henceforward, we shall focus on the lowest energy state with $\theta_1 = 0$, $\theta_2 = 2\pi/3$, $\theta_3 = -2\pi/3$, and $\phi_\alpha = \pi/2$, and study various electronic spectra.

Bogoliubov Fermi pockets.—As shown in Fig. 2(b), around the M and X points, $E(\mathbf{k})_1^+$ sinks down while $E(\mathbf{k})_1^-$ rises up, such that both of them go across zero energy. Indeed, this means that quasiparticles (holes) possess FSs, namely, Bogoliubov Fermi pockets come into being. These Fermi pockets are located at the M and X points and their periodic replica by the PDW (shifted by $\mathbf{q} = \pm\mathbf{Q}_\alpha \pm \mathbf{Q}_\beta \neq \mathbf{0}$), as indicated in Fig. 2(c). It is displayed in Fig. 2(d) that these Fermi pockets exhibit D_3 symmetry.

Density of states.—The differential conductance dI/dV measured by STM [37] is proportional to the DOS that reads $\rho(\omega) = -(1/8N)\sum_{\mathbf{k}}\sum_{i,j=1}^{16}\{|u(\mathbf{k})_{ij}|^2[\partial n_F(\omega - E(\mathbf{k})_j^+)/\partial\omega] + |v(\mathbf{k})_{ij}|^2[\partial n_F(\omega - E(\mathbf{k})_j^-)/\partial\omega]\}$, where n_F is the Fermi distribution, and $u(\mathbf{k})_{ij}$ and $v(\mathbf{k})_{ij}$ are found via Eq. (5). As demonstrated in Fig. 3, for $k_BT = \Delta/60 \ll \Delta$, $\rho(\omega)$ exhibits a minigap inside the SC gap manifested by sharp coherence peaks; while for $k_BT = \Delta/10 \lesssim \Delta$, $\rho(\omega)$ (thereby dI/dV) curve is of a V-shape. Note that both the minigap and the V-shaped DOS suggest electronic excitations inside the SC gap. The extra peaks outside sharp coherence peaks are attributed to the Van Hove singularity [38], and the asymmetry between $\rho(\omega)$ and $\rho(-\omega)$ is due to the broken particle-hole symmetry in $\xi_{\mathbf{k}}$.

Local density of states.—Now, we study the LDOS that serves as a standard tool to identify CDW orders by STM. The Fourier transformation of LDOS for the PDW state is given by $\rho(\mathbf{q},\omega) = -(1/8N)\sum_{\mathbf{k}}\sum_{i,j=1}^{16}\{u(\mathbf{k})_{ij}u^*(\mathbf{k}+\mathbf{q})_{ij}[\partial n_F(\omega - E(\mathbf{k})_j^+)/\partial\omega] + v(\mathbf{k})_{ij}v^*(\mathbf{k}+\mathbf{q})_{ij}[\partial n_F(\omega - E(\mathbf{k})_j^-)/\partial\omega]\}\bar{\delta}_{\mathbf{k},\mathbf{k}+\mathbf{q}}$, where $\bar{\delta}_{\mathbf{k},\mathbf{k}'} \equiv \sum_{n,m=-\infty}^{\infty}\delta_{\mathbf{k}+n\mathbf{Q}_1+m\mathbf{Q}_2,\mathbf{k}'}$ [35]. It has been found that $\rho(\mathbf{q},\omega)$ does not vanish only at a finite number of $\mathbf{q}$ points in the BZ, as labeled in Fig. 3(c). These $\mathbf{q}$ points are nothing but wave vectors of the descendant CDW order. Note that $|\rho(\mathbf{q},\omega)|$ takes the same value at $\mathbf{q}$ points within each set of B, C or D [35]. As demonstrated in Fig. 3(d), $|\rho(\mathbf{q},\omega)|$ displays both (B) 4×4 and (D) $4/\sqrt{3}\times4/\sqrt{3}$ CDW orders in addition to (C) 2×2 CDW order caused by the FS nesting. Define the integrated intensity of these CDW orders as $I_{\mathrm{CDW}}(\mathbf{q}) = |\int\rho(\mathbf{q},\omega)d\omega|/|\int\rho(\mathbf{q}=\mathbf{0},\omega)d\omega|$, we find that $I_{\mathrm{CDW}}^{B,C,D} = 1.51\times10^{-5}, 1.02\times10^{-5}, 2.82\times10^{-6}$ at $k_BT = \Delta/10$ for the three types of CDW orders, respectively.

Quasiparticle interference.—In the presence of elastic scatterings, the LDOS will be modulated due to the effect of QPI. To characterize this feature, we follow Ref. [39] to study the modulated LDOS $\delta\rho(\mathbf{r},\omega)$, or its Fourier transformation that is given by

$$\begin{aligned}&\delta\rho(\mathbf{q},\omega)\\&\equiv\rho_s(\mathbf{q},\omega)-\rho(\mathbf{q},\omega)\\&=-\frac{1}{16\pi N}\sum_{\mathbf{k}}\mathrm{Im}\tilde{\mathrm{Tr}}[\hat{\mathcal{G}}(\mathbf{k}+\mathbf{q},\omega+i\delta)\hat{T}(\omega)\hat{\mathcal{G}}(\mathbf{k},\omega+i\delta)],\end{aligned}\tag{9}$$

where ρ_s (ρ) is the LDOS in the presence (absence) of scatterings. $\tilde{\mathrm{Tr}}$ means tracing the upper-left 16×16 block in a 32×32 matrix. $\hat{\mathcal{G}}(\mathbf{k},\omega+i\delta) = [(\omega+i\delta)\mathcal{I} - \hat{\mathcal{H}}_{\mathbf{k}}]^{-1}$ is Green's function in the absence of scatterings and $\hat{T}(\omega) = [(V_s\hat{\tau}_3)^{-1} - (1/N)\sum_{\mathbf{k}}\hat{\mathcal{G}}(\mathbf{k},\omega+i\delta)]^{-1}$ is the scattering matrix. Here, V_s is the nonmagnetic scattering impurity strength, and $\hat{\tau}_3$ is the Pauli matrix spanning Nambu space.

The modulation $|\delta\rho(\mathbf{q},\omega)|$ with $V_s = 0.1$ at $\omega = 0.01(<\Delta = 0.02)$ is plotted in Fig. 4(a). For comparison, we also study QPI of a uniform s-wave superconductor, as shown in Fig. 4(b). In both figures, the intensity at $\mathbf{q} = \mathbf{0}$ has been subtracted.

Electron spectral function.—The LDOS modulation due to scatterings can be analyzed by electron spectral function $A(\mathbf{k},\omega) = -(1/\pi)\mathrm{Im}[\hat{\mathcal{G}}(\mathbf{k},\omega+i\delta)]_{11}$ in the absence of scattering. As is pointed out in Ref. [39], the summation in Eq. (9) is dominated by terms in which both $\mathbf{k}$ and $\mathbf{k}+\mathbf{q}$ are poles of $\hat{\mathcal{G}}$. Thus, the vectors $\mathbf{q}$ associated with the scattering processes connecting two points with large $A(\mathbf{k},\omega)$ will show significant $|\delta\rho(\mathbf{q},\omega)|$. This feature of $\mathbf{q}$ is displayed in Fig. 4(c). An essential difference between the PDW state and a uniform s-wave state is that the in-gap state is absent in the latter and the corresponding $A(\mathbf{k},\omega)$ and $|\delta\rho(\mathbf{q},\omega)|$ vanish at $\omega < \Delta$, as shown in Figs. 4(b)

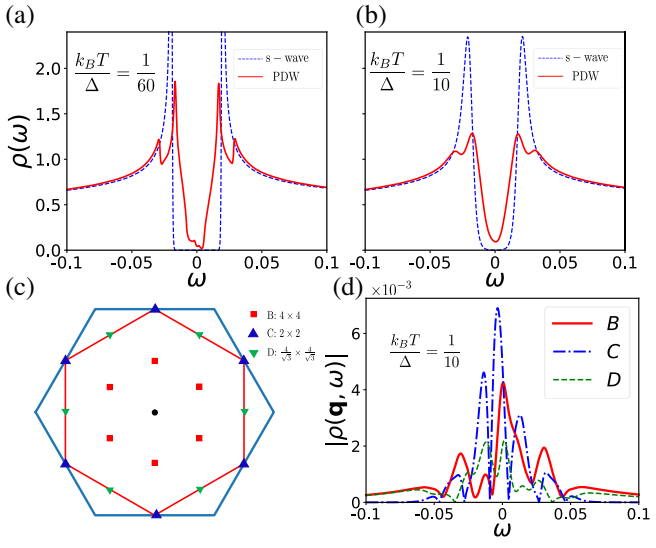

FIG. 3. DOS and LDOS. DOS $\rho(\omega)$ at (a) $k_BT/\Delta = 1/60$ and (b) $k_BT/\Delta = 1/10$. (c) Wave vectors $\mathbf{q} = \pm\mathbf{Q}_\alpha \pm \mathbf{Q}_\beta$ (or their equivalent vectors in first BZ) associated with descendant CDW orders. (d) LDOS $\rho(\mathbf{q},\omega)$ exhibits three types of CDW orders B, C, and D. Here, $\Lambda = 0.1$ and $\Delta = 0.02$ have been chosen.

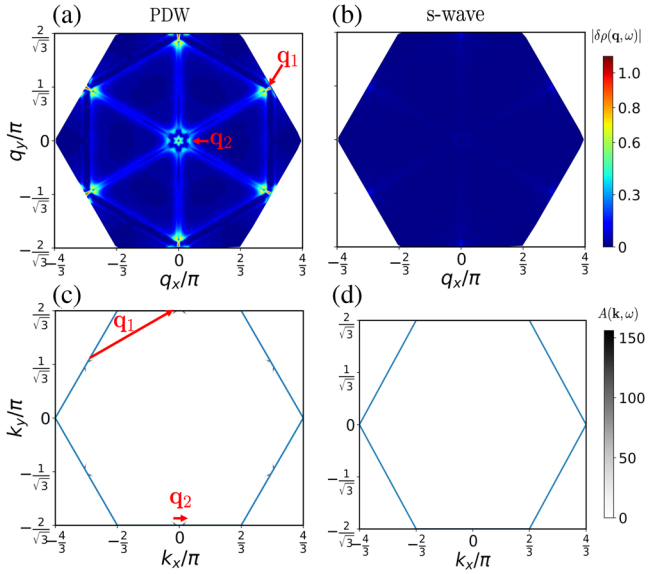

FIG. 4. LDOS modulation $|\delta\rho(\mathbf{q},\omega)|$ for (a) the PDW state and (b) a uniform s-wave SC state. Electron spectral function $A(\mathbf{k},\omega)$ for (c) the PDW state and (d) a uniform s-wave state. Wave vectors $\mathbf{q}_1$ and $\mathbf{q}_2$ in (a) and (c) indicate dominant scattering processes connecting two points with large $A(\mathbf{k},\omega)$ (and their symmetric equivalence). Here, $\omega = 0.01 < \Delta = 0.02$ has been chosen.

and 4(d). This also provides an experiment scheme to probe PDW states.

Discussions and conclusions.—(i) Recently discovered kagome SC AV_3Sb_5 (A = K,Rb,Cs) with a nearly 3/4 filled electron band is a natural platform toward the realization of the interplay between PDW and FS nesting [40–45]. TRS breaking signatures have been extensively discussed both experimentally and theoretically in AV_3Sb_5 [46–51]. For the SC properties, the AV_3Sb_5 is shown to be a spin-singlet SC hosting s-wave features [52–54]. However, a residual thermal transport at $T = 0$ and "multigap" V-shaped DOS with residual zero-energy contributions were observed in SC states [34,54–56], which conflicts with the conventional s-wave nature. This contradiction can be resolved within the TRS breaking PDW scenario proposed in the present Letter. More importantly, a PDW state ordering at $\mathbf{Q}_\alpha$ has been observed in recent STM measurements [34]. Therefore, our theory may provide new insight into the PDW states and TRS breaking in AV_3Sb_5. Indeed, both 2×2 and 4×4 CDWs have been observed in STM. Our theory suggests that the $(4/\sqrt{3}) \times (4/\sqrt{3})$ CDW should appear as well, as long as the frequency ω is chosen properly.

(ii) Indeed, such a TRS breaking SC state breaks the spatial inversion symmetry as well [see Eq. (2)], resulting in a chiral state with stable residual gapless quasiparticle excitations. The ground state is a flux state with spontaneous loop current [57,58], as calculated in the Supplemental Material [35]. And the Bogoliubov Fermi pockets yield the linear T-dependent specific heat at low temperature.

(iii) One of the remaining issues is what microscopic theory may give rise to the finite-momentum Cooper pairing instability on a nested FS. In the weak interaction limit, pairing at zero momentum is usually favored. Nonetheless, strong correlation might favor PDW instability against uniform pairing (see, e.g., Refs. [15,59]). By establishing the microscopic model, the comparison with relevant models [60–63] based on the conventional CDW instabilities with nesting vector $2\mathbf{Q}_\alpha$ is one of the essential topics.

In summary, we have found that the FS nesting allows a full PDW pairing and in-gap states simultaneously. Such a PDW ansatz will give rise to a TRS breaking ground state. Subsequently, descendant CDW orders and various electronic spectra have been studied, and the relevance to newly discovered kagome SC has been revealed.

This work is partially supported by the National Natural Science Foundation of China (Grants No. 12274441, No. 12034004, No. 12174428, and No. 11825404), National Basic Research Program of China (Grant No. 2018YFA0305604 and No. 2021YFA1400100), the K. C. Wong Education Foundation (Grant No. GJTD-2020-01), Beijing Natural Science Foundation (Grant No. Z180010), and the Strategic Priority Research Program of Chinese Academy of Sciences (Grant No. XDB28000000).

*jiangkun@iphy.ac.cn
†yaohong@tsinghua.edu.cn
‡yizhou@iphy.ac.cn

[1] E. Berg, E. Fradkin, E.-A. Kim, S. A. Kivelson, V. Oganesyan, J. M. Tranquada, and S. C. Zhang, Dynamical Layer Decoupling in a Stripe-Ordered High-T_c Superconductor, Phys. Rev. Lett. **99**, 127003 (2007).
[2] D. Agterberg and H. Tsunetsugu, Dislocations and vortices in pair-density-wave superconductors, Nat. Phys. **4**, 639 (2008).
[3] E. Berg, E. Fradkin, S. A. Kivelson, and J. M. Tranquada, Striped superconductors: How spin, charge and superconducting orders intertwine in the cuprates, New J. Phys. **11**, 115004 (2009).
[4] E. Berg, E. Fradkin, and S. A. Kivelson, Pair-Density-Wave Correlations in the Kondo-Heisenberg Model, Phys. Rev. Lett. **105**, 146403 (2010).
[5] A. Jaefari and E. Fradkin, Pair-density-wave superconducting order in two-leg ladders, Phys. Rev. B **85**, 035104 (2012).
[6] G. Y. Cho, J. H. Bardarson, Y.-M. Lu, and J. E. Moore, Superconductivity of doped Weyl semimetals: Finite-momentum pairing and electronic analog of the ^{3}He-A phase, Phys. Rev. B **86**, 214514 (2012).
[7] R. Soto-Garrido and E. Fradkin, Pair-density-wave superconducting states and electronic liquid-crystal phases, Phys. Rev. B **89**, 165126 (2014).

[8] P. A. Lee, Amperean Pairing and the Pseudogap Phase of Cuprate Superconductors, Phys. Rev. X **4**, 031017 (2014).

[9] J. Maciejko and R. Nandkishore, Weyl semimetals with short-range interactions, Phys. Rev. B **90**, 035126 (2014).

[10] Y. Wang, D. F. Agterberg, and A. Chubukov, Coexistence of Charge-Density-Wave and Pair-Density-Wave Orders in Underdoped Cuprates, Phys. Rev. Lett. **114**, 197001 (2015).

[11] S.-K. Jian, Y.-F. Jiang, and H. Yao, Emergent Spacetime Supersymmetry in 3D Weyl Semimetals and 2D Dirac Semimetals, Phys. Rev. Lett. **114**, 237001 (2015).

[12] S.-K. Jian, C.-H. Lin, J. Maciejko, and H. Yao, Emergence of Supersymmetric Quantum Electrodynamics, Phys. Rev. Lett. **118**, 166802 (2017).

[13] Y. Wang, S. D. Edkins, M. H. Hamidian, J. C. Seamus Davis, E. Fradkin, and S. A. Kivelson, Pair density waves in superconducting vortex halos, Phys. Rev. B **97**, 174510 (2018).

[14] J. Venderley and E.-A. Kim, Evidence of pair-density wave in spin-valley locked systems, Sci. Adv. **5**, eaat4698 (2019).

[15] Z. Han, S. A. Kivelson, and H. Yao, Strong Coupling Limit of the Holstein-Hubbard Model, Phys. Rev. Lett. **125**, 167001 (2020).

[16] K. Slagle and L. Fu, Charge transfer excitations, pair density waves, and superconductivity in moiré materials, Phys. Rev. B **102**, 235423 (2020).

[17] S. Zhou and Z. Wang, Chern Fermi-pockets and chiral topological pair density waves in kagome superconductors, arXiv:2110.06266.

[18] K. S. Huang, Z. Han, S. A. Kivelson, and H. Yao, Pair-density-wave in the strong coupling limit of the holstein-hubbard model, npj Quantum Mater. **7**, 17 (2022).

[19] Y.-M. Wu, Z. Wu, and H. Yao, Pair-density-wave and chiral superconductivity in twisted bilayer transition-metal-dichalcogenides, arXiv:2203.05480.

[20] D. F. Agterberg, J. S. Davis, S. D. Edkins, E. Fradkin, D. J. Van Harlingen, S. A. Kivelson, P. A. Lee, L. Radzihovsky, J. M. Tranquada, and Y. Wang, The physics of pair-density waves: Cuprate superconductors and beyond, Annu. Rev. Condens. Matter Phys. **11**, 231 (2020).

[21] P. Fulde and R. A. Ferrell, Superconductivity in a strong spin-exchange field, Phys. Rev. **135**, A550 (1964).

[22] A. I. Larkin and Y. N. Ovchinnikov, Quasiclassical method in the theory of superconductivity, Sov. Phys. JETP **28**, 1200 (1969).

[23] R. Casalbuoni and G. Nardulli, Inhomogeneous superconductivity in condensed matter and QCD, Rev. Mod. Phys. **76**, 263 (2004).

[24] M. H. Hamidian, S. D. Edkins, S. H. Joo, A. Kostin, H. Eisaki, S. Uchida, M. J. Lawler, E.-A. Kim, A. P. Mackenzie, K. Fujita, J. Lee, and J. C. S. Davis, Detection of a cooper-pair density wave in $Bi_2Sr_2CaCu_2O_{8+x}$, Nature (London) **532**, 343 (2016).

[25] W. Ruan, X. Li, C. Hu, Z. Hao, H. Li, P. Cai, X. Zhou, D.-H. Lee, and Y. Wang, Visualization of the periodic modulation of Cooper pairing in a cuprate superconductor, Nat. Phys. **14**, 1178 (2018).

[26] S. D. Edkins, A. Kostin, K. Fujita, A. P. Mackenzie, H. Eisaki, S. Uchida, S. Sachdev, M. J. Lawler, E.-A. Kim, J. C. S. Davis, and M. H. Hamidian, Magnetic field-induced pair density wave state in the cuprate vortex halo, Science **364**, 976 (2019).

[27] X. Li, C. Zou, Y. Ding, H. Yan, S. Ye, H. Li, Z. Hao, L. Zhao, X. Zhou, and Y. Wang, Evolution of Charge and Pair Density Modulations in Overdoped $Bi_2Sr_2CuO_{6+\delta}$, Phys. Rev. X **11**, 011007 (2021).

[28] R. E. Peierls, *Quantum Theory of Solids* (Oxford University, New York, 1955).

[29] H. Fröhlich, On the theory of superconductivity: the one-dimensional case, Proc. R. Soc. A **223**, 296 (1954).

[30] G. Grüner, The dynamics of charge-density waves, Rev. Mod. Phys. **60**, 1129 (1988).

[31] A. W. Overhauser, Giant Spin Density Waves, Phys. Rev. Lett. **4**, 462 (1960).

[32] A. W. Overhauser, Spin density waves in an electron gas, Phys. Rev. **128**, 1437 (1962).

[33] G. Grüner, The dynamics of spin-density waves, Rev. Mod. Phys. **66**, 1 (1994).

[34] H. Chen *et al.*, Roton pair density wave in a strong-coupling kagome superconductor, Nature (London) **599**, 222 (2021).

[35] See Supplemental Material at http://link.aps.org/supplemental/10.1103/PhysRevLett.129.167001 for more details.

[36] J. R. Schrieffer, *Theory of Superconductivity* (Westview Press, Nashville, Tennessee, 1999).

[37] G. Binnig and H. Rohrer, Scanning tunneling microscopy—from birth to adolescence, Rev. Mod. Phys. **59**, 615 (1987).

[38] L. Van Hove, The occurrence of singularities in the elastic frequency distribution of a crystal, Phys. Rev. **89**, 1189 (1953).

[39] Q.-H. Wang and D.-H. Lee, Quasiparticle scattering interference in high-temperature superconductors, Phys. Rev. B **67**, 020511(R) (2003).

[40] B. R. Ortiz, S. M. L. Teicher, Y. Hu, J. L. Zuo, P. M. Sarte, E. C. Schueller, A. M. Milinda Abeykoon, M. J. Krogstad, S. Rosenkranz, R. Osborn, R. Seshadri, L. Balents, J. He, and S. D. Wilson, CsV_3Sb_5: A F_2 Topological Kagome Metal with a Superconducting Ground State, Phys. Rev. Lett. **125**, 247002 (2020).

[41] B. R. Ortiz, P. M. Sarte, E. M. Kenney, M. J. Graf, S. M. L. Teicher, R. Seshadri, and S. D. Wilson, Superconductivity in the F_2 kagome metal KV_3Sb_5, Phys. Rev. Mater. **5**, 034801 (2021).

[42] Q. Yin, Z. Tu, C. Gong, Y. Fu, S. Yan, and H. Lei, Superconductivity and normal-state properties of kagome metal RbV_3Sb_5 single crystals, Chin. Phys. Lett. **38**, 037403 (2021).

[43] K. Jiang, T. Wu, J.-X. Yin, Z. Wang, M. Z. Hasan, S. D. Wilson, X. Chen, and J. Hu, Kagome superconductors AV_3Sb_5 (A = K, Rb, Cs), arXiv:2109.10809.

[44] B. R. Ortiz, S. M. L. Teicher, L. Kautzsch, P. M. Sarte, N. Ratcliff, J. Harter, J. P. C. Ruff, R. Seshadri, and S. D. Wilson, Fermi Surface Mapping and the Nature of Charge-Density-Wave Order in the Kagome Superconductor CsV_3Sb_5, Phys. Rev. X **11**, 041030 (2021).

[45] F. Kaboudvand, S. M. L. Teicher, S. D. Wilson, R. Seshadri, and M. D. Johannes, Fermi surface nesting and the Lindhard response function in the kagome superconductor CsV_3Sb_5, Appl. Phys. Lett. **120**, 111901 (2022).

[46] Y.-X. Jiang, J.-X. Yin, M. M. Denner, N. Shumiya, B. R. Ortiz, G. Xu, Z. Guguchia, J. He, M. S. Hossain, X. Liu *et al.*, Unconventional chiral charge order in kagome superconductor KV_3Sb_5, Nat. Mater. **20**, 1353 (2021).

[47] L. Yu, C. Wang, Y. Zhang, M. Sander, S. Ni, Z. Lu, S. Ma, Z. Wang, Z. Zhao, H. Chen, K. Jiang, Y. Zhang, H. Yang, F. Zhou, X. Dong, S. L. Johnson, M. J. Graf, J. Hu, H.-J. Gao, and Z. Zhao, Evidence of a hidden flux phase in the topological kagome metal CsV_3Sb_5, arXiv:2107.10714.

[48] C. Mielke III *et al.*, Time-reversal symmetry-breaking charge order in a kagome superconductor, Nature (London) **602**, 245 (2022).

[49] X. Feng, K. Jiang, Z. Wang, and J. Hu, Chiral flux phase in the kagome superconductor AV_3Sb_5, Sci. Bull. **66**, 1384 (2021).

[50] Y.-P. Lin and R. M. Nandkishore, Complex charge density waves at Van Hove singularity on hexagonal lattices: Haldane-model phase diagram and potential realization in the kagome metals aV_3sb_5 ($A = $ K, Rb, Cs), Phys. Rev. B **104**, 045122 (2021).

[51] T. Park, M. Ye, and L. Balents, Electronic instabilities of kagome metals: Saddle points and landau theory, Phys. Rev. B **104**, 035142 (2021).

[52] C. Mu, Q. Yin, Z. Tu, C. Gong, H. Lei, Z. Li, and J. Luo, S-wave superconductivity in kagome metal CsV_3Sb_5 revealed by $^{121/123}$Sb NQR and ^{51}V NMR measurements, Chin. Phys. Lett. **38**, 077402 (2021).

[53] W. Duan, Z. Nie, S. Luo, F. Yu, B. R. Ortiz, L. Yin, H. Su, F. Du, A. Wang, Y. Chen, X. Lu, J. Ying, S. D. Wilson, X. Chen, Y. Song, and H. Yuan, Nodeless superconductivity in the kagome metal CsV_3Sb_5, Sci. China Phys. Mech. Astron. **64**, 107462 (2021).

[54] H.-S. Xu, Y.-J. Yan, R. Yin, W. Xia, S. Fang, Z. Chen, Y. Li, W. Yang, Y. Guo, and D.-L. Feng, Multiband Superconductivity with Sign-Preserving Order Parameter in Kagome Superconductor CsV_3Sb_5, Phys. Rev. Lett. **127**, 187004 (2021).

[55] C. C. Zhao, L. S. Wang, W. Xia, Q. W. Yin, J. M. Ni, Y. Y. Huang, C. P. Tu, Z. C. Tao, Z. J. Tu, C. S. Gong, H. C. Lei, Y. F. Guo, X. F. Yang, and S. Y. Li, Nodal superconductivity and superconducting domes in the topological kagome metal CsV_3Sb_5, arXiv:2102.08356.

[56] Z. Liang, X. Hou, F. Zhang, W. Ma, P. Wu, Z. Zhang, F. Yu, J.-J. Ying, K. Jiang, L. Shan, Z. Wang, and X.-H. Chen, Three-Dimensional Charge Density Wave and Surface-Dependent Vortex-Core States in a Kagome Superconductor CsV_3Sb_5, Phys. Rev. X **11**, 031026 (2021).

[57] J. P. Rodriguez and B. Douçot, Superconductivity, Faraday effect, and optical absorption in the commensurate flux phase of the *t*-*J* model, Phys. Rev. B **45**, 971 (1992).

[58] D. F. Agterberg, D. S. Melchert, and M. K. Kashyap, Emergent loop current order from pair density wave superconductivity, Phys. Rev. B **91**, 054502 (2015).

[59] M. Zegrodnik and J. Spałek, Incorporation of charge- and pair-density-wave states into the one-band model of *d*-wave superconductivity, Phys. Rev. B **98**, 155144 (2018).

[60] C. Honerkamp, Instabilities of interacting electrons on the triangular lattice, Phys. Rev. B **68**, 104510 (2003).

[61] W.-S. Wang, Z.-Z. Li, Y.-Y. Xiang, and Q.-H. Wang, Competing electronic orders on kagome lattices at van Hove filling, Phys. Rev. B **87**, 115135 (2013).

[62] R. Nandkishore, R. Thomale, and A. V. Chubukov, Superconductivity from weak repulsion in hexagonal lattice systems, Phys. Rev. B **89**, 144501 (2014).

[63] Y.-P. Lin and R. M. Nandkishore, Multidome superconductivity in charge density wave kagome metals, Phys. Rev. B **106**, L060507 (2022).